Numerical analysis of surface plasmon nanocavities formed in thickness-modulated metal–insulator–metal waveguides*

Liu Jian-Long(刘建龙)[a], Lin Jie(林 杰)[b], Zhao Hai-Fa(赵海发)[a], Zhang Yan(张 岩)[c], and Liu Shu-Tian(刘树田)[a]†

[a] *Department of Physics, Harbin Institute of Technology, Harbin* 150001, *China*
[b] *School of Electrical Engineering and Automation, Harbin Institute of Technology, Harbin* 150001, *China*
[c] *Department of Physics, Capital Normal University, Beijing* 100037, *China*

(Received 30 May 2009; revised manuscript received 18 September 2009)

The enhancement characteristics of the local field in the surface plasmon nanocavities are investigated numerically. The cavity is constructed by placing a defect structure in the thickness-modulated metal–insulator–metal waveguide Bragg gratings. The characteristic impedance based transfer matrix method is used to calculate the transmission spectra and the resonant wavelength of the cavities with various geometric parameters. The finite-difference time-domain method is used to obtain the field pattern of the resonant mode and validate the results of the transfer matrix method. The calculation and simulation results reveal the existence of resonant wavelength shift and intensity variation with structural parameters, such as the modulation period of the gratings, the length and the width of the defect structure. Both numerical analysis and theoretical interpretation on these phenomena are given in details.

Keywords: surface plasmon, nanocavity, local field enhancement
PACC: 4200, 7340R, 4280L

1. Introduction

Diffraction limit is one of the major problems in modern photonics when the electromagnetic waves are focused on the subwavelength dimension.[1,2] It brings a great barrier in the development of miniaturization of optical devices and the integration of photonic circuits. One way to overcome the diffraction limit and achieve the subwavelength localization of electromagnetic waves is to constraint light in metallic nano-scale structures with the help of surface plasmon polariton (SPP).[3–5]

SPP is a special kind of electromagnetic field that can be confined at the metallic surface. In recent years, various plasmonic elements have been proposed to realize the propagation, the concentration and the modulation of the electromagnetic waves in subwavelength scale.[6–17] Among them, the metal–insulator–metal (MIM) waveguides[13–17] and MIM based devices are considered to possess remarkable advantages in the practical applications, such as easy fabrication and integration into optical circuits. For the potential applications in SPP-emitting devices[18] and SPP-based lasers[19] on the nano scale, the cavities constructed in MIM waveguides have attracted much attention. Wang and Wang[20] proposed a metal heterostructure SPP Bragg reflector constructed by alternately stacking two kinds of MIM waveguides with different metallic materials. A nanocavity structure was formed by introducing a defect in the middle of the Bragg reflector. However, the dielectric constants of low loss metals (such as Ag, Au and Cu) are not distinguishable enough to produce an effective contrast which is required to realize wide Bragg reflectors and high Q-value cavities. Hosseini and Massoud[21] suggested another cavity structure by periodically varying the dielectric materials of the insulator. However, filling dielectric materials in the waveguide will increase the Ohmic loss due to the damping of electrons in the metal. After that, Han *et al.*[22] proposed a surface plasmon nanocavity structure formed in periodic thickness-modulated MIM waveguides. By changing the insulator thickness, the effective refractive index of the waveguide can be tuned continuously. This convenience is impossible to be presented in the former two methods. However, the optical characteristics of

*Project supported by the National Natural Science Foundation of China (Grant Nos. 10674038 and 10604042), and the National Basic Research Program of China (Grant No. 2006CB302901).
†Corresponding author. E-mail: stliu@hit.edu.cn
© 2010 Chinese Physical Society and IOP Publishing Ltd

this kind of surface plasmon cavity could be sensitive to the geometric parameters of the structure. It is necessary to have a systematic analysis of the influence of these parameters on the performance of the nanocavities formed in thickness-modulated MIM waveguides. This paper focuses on this issue.

More recently, Hu *et al.*[23] reported on an enhanced effect of local fields in the two-dimensional subwavelength-size metallic series nanocavities. The structure in their work possessed a continuous varying thickness of the insulator and a narrow channel in the middle as a cavity. It is shown that the amplitude of local magnetic field in the middle narrow channel can be enhanced up to 2 orders of magnitude of the incident light field at the resonant wavelength. The SPP on the metal is declared to play a critical role for this enhancement phenomenon. However, the mechanism of the excitation of the SPP resonant mode remains unclear in Ref. [23]. The uncertainties of the reason for the resonant wavelength shift which was reported in Ref. [23], still exist. In our paper, we will try to give a more reasonable explanation to these phenomena.

Based on these reasons, this paper focuses on the systematic investigations of enhancement and concentration phenomena and the theoretical analysis of the mechanism of the resonant mode in the nanocavity which is constructed in the thickness-modulated MIM waveguides. The detailed numerical analysis about the influence of various geometric parameters on the optical characteristics of the cavity structure is given. The characteristic impedance based transfer matrix method (TMM) is used to calculate the transmission spectra and the resonant wavelength of the cavity structure. The finite-difference time-domain (FDTD) method is used to obtain the field pattern of the resonant mode and validate the TMM results.

2. Transfer matrix model

The structure we discuss in this paper is sketched in Fig. 1, which is a thickness-modulated MIM waveguide Bragg grating containing a defect structure in the centre. Our study is focused on the modes of propagation in the longitudinal x direction. Therefore the metals are presumed to be thick enough in the transverse y direction. The whole structure can be represented by $(\mathrm{AB})^N\mathrm{C}(\mathrm{BA})^N$ where A and B are the MIM waveguides with insulator thicknesses d_A and d_B, N denotes the period number of AB part, and C, which is localized in the centre, is the cavity with length l_C and insulator thickness d_A.

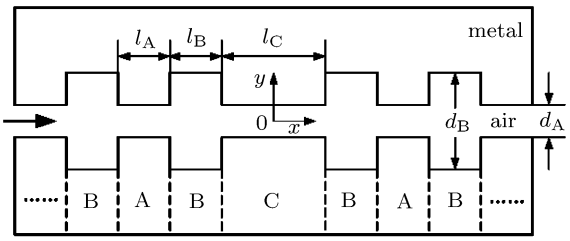


Fig. 1. Schematic diagram of 2D nanocavity formed in thickness-modulated MIM waveguides.

Firstly we review the properties of SPP in the MIM waveguides. When the thickness of the insulator layer is reduced below the diffraction limit, the conventional guiding modes cannot exist. It has been demonstrated that only a surface plasmon mode TM_0, where E_z, H_x and H_y are identically zero, can exist in an extremely narrow waveguide.[17] Assuming all components of the electromagnetic fields propagating in the x-direction to take the form of $\exp[\mathrm{i}(\omega t - \beta x)]$, the dispersion equation for TM_0 mode can be written as

$$\tanh\left(\frac{\sqrt{\beta^2 - k_0^2\varepsilon_\mathrm{i}}d}{2}\right) = \frac{-\varepsilon_\mathrm{i}\sqrt{\beta^2 - k_0^2\varepsilon_\mathrm{m}}}{\varepsilon_\mathrm{m}\sqrt{\beta^2 - k_0^2\varepsilon_\mathrm{i}}}, \qquad (1)$$

where k_0 is the wave number of light in the free space, β is the longitudinal wave number which can be written as $\beta = n^{\mathrm{eff}}k_0$ (n^{eff} is the effective refraction index in the waveguide), ε_i and ε_m are dielectric functions of insulator and metallic material respectively. The insulator in this paper is assumed to be air with a permittivity of $\varepsilon_\mathrm{i} = 1$ and silver is used for the metal layers characterized by the Drude model

$$\varepsilon_\mathrm{m}(\omega) = \varepsilon_\infty - \frac{\omega_\mathrm{p}^2}{\omega(\omega + \mathrm{i}\,\gamma)}, \qquad (2)$$

where ε_∞ represents the dielectric constant at infinite frequency, ω_p denotes the bulk plasmon frequency, γ means the oscillation damping of electrons, and ω is the frequency of the incident light. We find $\varepsilon_\infty = 3.71$, $\omega_\mathrm{p} = 1.38 \times 10^{16}$ rad/s , $\gamma = 2.73 \times 10^{13}$ rad/s to be able to provide a good description of empirical dielectric constant data for silver over a wide range of wavelength.[24]

If the dimension of the waveguide structure is smaller than that of the wavelength, the quasi-static approximation[25] holds and the stacked waveguide structure can be considered as a transmission line[26−28] which is a useful concept in microwave network theory. When the waveguide dimensions are in a

deep subwavelength range, the definition for the characteristic impedance of such a waveguide transmission line can be written as

$$Z = \frac{\beta d}{\omega \varepsilon_{\rm i}}, \tag{3}$$

where ω is the incident frequency and d is the insulator thickness of the waveguide. Under such circumstances, the transmission characteristic of the structure depicted in Fig. 1 can be described by using the characteristic impedance based transfer matrix formalism $\boldsymbol{M}$. For a single ABA structure, the matrix $\boldsymbol{M}$ can be written as

$$\boldsymbol{M} = \begin{pmatrix} M_{11} & M_{12} \\ M_{21} & M_{22} \end{pmatrix} = \boldsymbol{D}_{\rm A}^{-1}\boldsymbol{D}_{\rm B}\boldsymbol{P}_{\rm B}\boldsymbol{D}_{\rm B}^{-1}\boldsymbol{D}_{\rm A}, \tag{4}$$

where

$$\boldsymbol{D}_{\rm A,B} = \begin{pmatrix} 1 & 1 \\ 1/\boldsymbol{Z}_{\rm A,B} & -1/\boldsymbol{Z}_{\rm A,B} \end{pmatrix}, \tag{5}$$

$$\boldsymbol{P}_{\rm B} = \begin{pmatrix} \exp(\mathrm{i}\,\beta_{\rm B}^{*} l_{\rm B}) & 0 \\ 0 & \exp(-\mathrm{i}\,\beta_{\rm B}^{*} l_{\rm B}) \end{pmatrix}. \tag{6}$$

$\boldsymbol{D}_{\rm A}^{-1}\boldsymbol{D}_{\rm B}$ is the transfer matrix at the junction between A and B, $\boldsymbol{P}_{\rm B}$ is the propagation matrix which accounts for the propagation through the bulk of the waveguide, and symbol * is the conjugate operation. Since the bounding structures are both waveguide A, the energy transmission T is given by $T = |t|^2 = |1/M_{11}|^2$. The transfer matrix $\boldsymbol{M}$ for other forms of stacked structures can be deduced analogously.

To demonstrate the validity of expression (4), we use both TMM and FDTD methods to calculate the energy transmission of the single ABA structure. The parameters are chosen to be $d_{\rm A} = 50$ nm, $d_{\rm B} = 150$ nm, and $l_{\rm B} = 1500$ nm. The FDTD simulation is performed by using uniform Yee cell of $\Delta x = \Delta y = 2$ nm. From the result, which is depicted in Fig. 2, the TMM calculation and FDTD simulation are in good agreement especially at the transmission peaks. The main differences only exist at the valley points. Fortunately, this deviation decreases with the increase of wavelength, which is in accordance with the quasi-static approximation we used in TMM calculation.

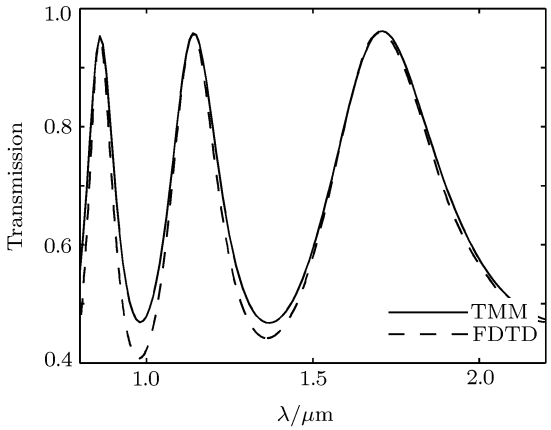


Fig. 2. Transmission spectra of a single ABA structure with parameters $d_{\rm A} = 50$ nm, $d_{\rm B} = 150$ nm, and $l_{\rm B} = 1500$ nm calculated by TMM and FDTD method respectively.

TMM is a useful systematic approach to the analysis of the electromagnetic waves propagating in layered media. Unlike FDTD method which requires heavy computation effort, TMM can extract transmission and reflection spectrum directly after the transfer matrix has been determined.[29] It is especially useful when a large portion of the structure is periodic. In the following section, we will use TMM to calculate the spectra of the designed structures and use FDTD method to obtain the field distribution of the resonant mode in the cavity and verify the resonant wavelength.

3. Numerical analysis and results

As depicted in Fig. 1, the cavity can be constructed by placing two identical high reflectance MIM Bragg reflectors on both the left- and the right-hand sides to form a Fabry–Pérot-like structure. The Bragg reflector structure consists of alternating quarter-wave waveguides with different insulator thicknesses. Such a Bragg reflector can be described by using $(\mathrm{BA})^N$, where N denotes the repeating number. The Bragg wavelength is set to be 1550 nm which is in the L-band of optical telecommunications. The insulator thicknesses of waveguides A and B are set to be 50 nm and 150 nm. Using the dispersion equation (1), the effective refractive indices of two sections can be obtained: $n_{\rm A}^{\rm eff} = 1.3755 + 0.0038\,\mathrm{i}$ and $n_{\rm B}^{\rm eff} = 1.1395 + 0.0015\,\mathrm{i}$ at $\lambda_{\rm b} = 1550$ nm. According to the quarter-wave condition $l_{\rm A}\mathrm{Re}(n_{\rm A}^{\rm eff}) = \lambda_{\rm b}/4$ and $l_{\rm B}\mathrm{Re}(n_{\rm B}^{\rm eff}) = \lambda_{\rm b}/4$, we can realize Bragg reflectance by choosing the waveguide length as $l_{\rm A} = 282$ nm and $l_{\rm B} = 340$ nm.

Figure 3 shows the energy reflectance spectra and the phase shift during the reflection for the Bragg structure $(BA)^N$ with $N = 1$, 2, 3 and 4. It illustrates that an obvious forbidden band exists around the Bragg wavelength 1550 nm. As the period number N increases, the peak reflectance approaches unity. It implies that the thickness modulated MIM waveguide Bragg reflector can provide a high reflectance so that it can be used to construct a Fabry–Pérot-like cavity structure. Unlike the reflection of metallic mirror, however, Bragg reflection is strongly associated with a phase dispersion, which is depicted in Fig. 3(b). The phase shift changes slowly around the central wavelength, but rapidly at the wavelength outside the forbidden band. It is worth noting that the phase shift is fixed at 0 at the Bragg wavelength λ_B no matter how N changes. But for the other wavelengths on the right- and the left-hand sides, the phase shift drifts oppositely as N decreases, and it is especially obvious for $N = 1$. This is clearly illustrated in the inset of Fig. 3(b).

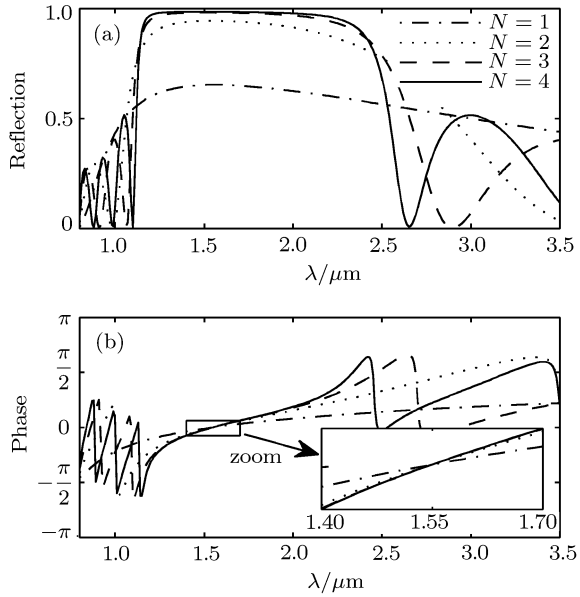


Fig. 3. Energy reflection (a) and the phase shift (b) spectra of a N-period Bragg reflector $(BA)^N$, where $N = 1$, 2, 3 and 4. Other parameters are $d_A = 50$ nm and $d_B = 150$ nm.

In order to construct a nanocavity with a resonant wavelength located in the centre of the forbidden band, a defect layer C is constructed by repeating the waveguide A twice: $l_C = 2l_A = 564$ nm. The whole structure can be described by using $(AB)^N A^2 (BA)^N$. The transmission spectra of the structures with $N = 1$, 2, 3 and 4 are depicted in Fig. 4. It can be seen that a transmission maximum occurs in Bragg wavelength $\lambda_B = 1550$ nm, which means that an SPP resonant defect mode is excited in the cavity. This can be well interpreted by using the Fabry–Pérot resonant condition equation

$$2k_0 n_C^{\text{eff}} l_C = \phi_L + \phi_R + 2m\pi, \tag{7}$$

where k_0 is the wave number in the free space: $k_0 = 2\pi/\lambda$, n_C^{eff} is the effective refractive index in layer C, l_C is the cavity length, $\phi_L$and ϕ_R are the phase shifts caused by the reflection on the left- and right-hand sides of the cavity respectively, and m is an integral number. The resonant condition is satisfied exactly at the Bragg wavelength λ_B since the cavity layer C is constructed by stacking two quarter-wave layers and the phase shifts ϕ_L and ϕ_R, which are shown clearly in Fig. 3(b), are identically zero.

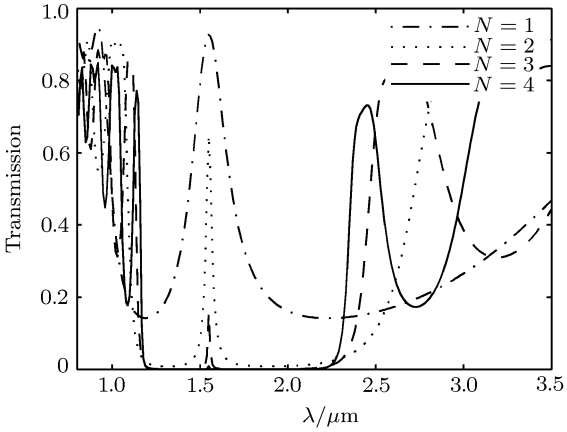


Fig. 4. Transmission spectra of cavity structure $(AB)^N A^2 (BA)^N$ described in Fig. 1. The insulator thicknesses of waveguide A and B are the same as those in Fig. 3.

The quality factor $Q = \lambda/\Delta\lambda$, which describes the lifetime of the resonant mode, is also calculated. For the cases of $N = 1$, 2, 3 and 4, the Q values are 6, 39, 126, and 191, respectively. This result indicates that the value of Q increases significantly with the number of periods increasing. The oscillations in the cavity will die out more slowly at higher Q values which indicates a lower rate of energy dissipation. To illustrate how the energy is conserved in the central cavity, the $|H_z|^2$ distributions at incident wavelength $\lambda = 1550$ nm in the waveguide with different values of N are displayed in Fig. 5. It can be seen that a bright spot exists in the centre and a dark zone surrounds it, which indicates that the SPP is localized strongly in the cavity. The corresponding longitudinal cross sections of the local fields in the cavity along x-axis are depicted in Fig. 6. It can be seen that the field

intensity in the centre of the cavity is enhanced several times as high as that of the incident light. The peak value of the intensity reaches its maximum at $N = 3$ and falls back when $N = 4$ even though it possesses the highest Q value. This phenomenon is also reported in Ref. [23], but without enough interpretation. The decline of the field enhancement for a larger period number is mainly due to the increasing of heat loss from the metal and the end fire excitation method used in these cases.

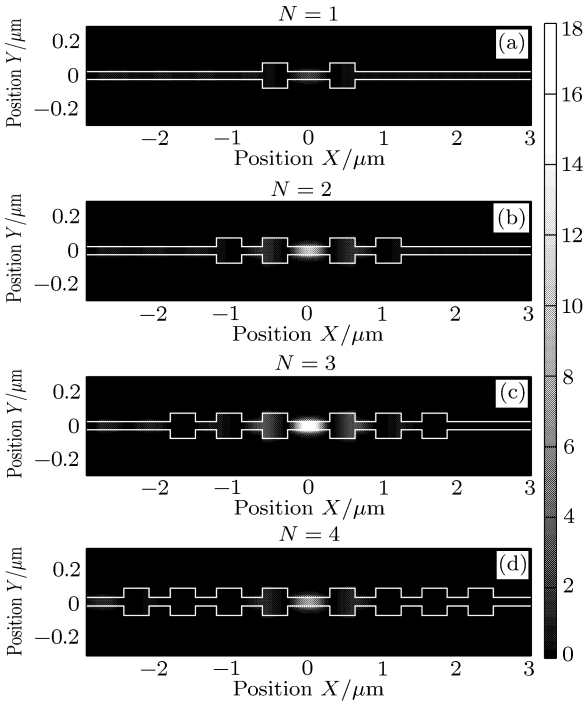


Fig. 5. Intensity $|H_z|^2$ distributions inside cavity with 1(a), 2(b), 3(c) and 4(d) periods of Bragg cells. The incident wavelength is fixed at 1550 nm.

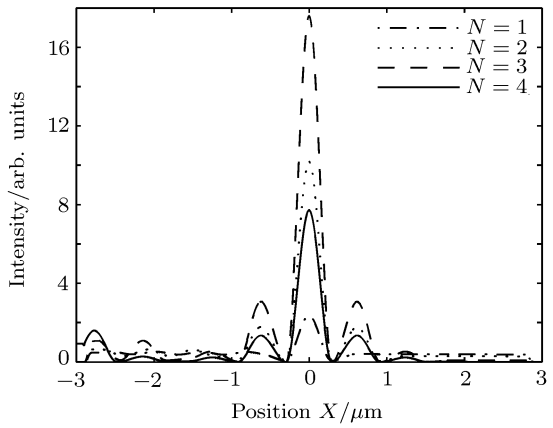


Fig. 6. $|H_z|^2$ profiles along x-axis on line $y = 0$.

For comparison, the lossless cases, in which the imaginary part of the permittivity of silver is ignored, are also simulated and shown in Fig. 7. Comparing with the loss cases in Fig. 6, the enhancement is strong, especially for $N = 4$ case in which the peak value returns back to the highest. This accords well with the highest Q value for $N = 4$.

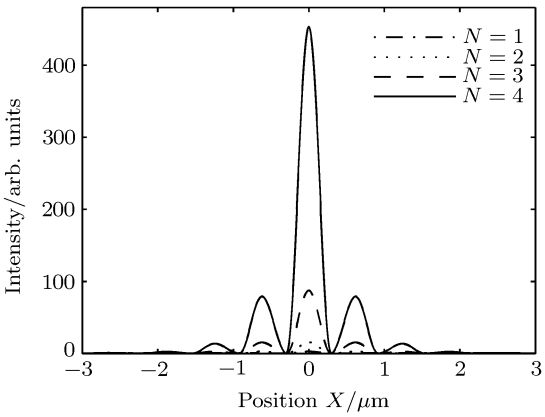


Fig. 7. $|H_z|^2$ profiles along x-axis on line $y = 0$ for lossless cases.

As a resonant cavity, the resonant wavelength could be tuned by changing the length of cavity. To explore the influence of the defect layer length l_C on resonant property, we increase and reduce the length from $l_C = 564$ nm to $l_C = 650$ nm and $l_C = 450$ nm, respectively. Other parameters remain unchanged. The transmission spectra are depicted in Fig. 8. To show the position of the resonant wavelength more clearly, the wavelength range of the spectrum is reduced to [1200, 2000] nm which just falls in the forbidden band of the Bragg grating. It is clearly seen that with the increase and the decrease of the length of defect layer, the resonant wavelength peak is red-shifted and blue-shifted respectively. This can be well understood by using expression (7). The phase shifts ϕ_L and ϕ_R are independent of cavity length. In order to maintain the resonant condition, a longer or shorter wavelength is required for increasing or decreasing cavity length l_C. It is also worth noting that the resonant wavelength in the case of $l_C = 650$ nm is red-shifted when N decreases to 1. This phenomenon was also reported in Ref. [23]. But the blue-shift, which is obvious for $l_C = 450$ nm when $N = 1$, is not mentioned in their work. This phenomenon of resonant wavelength shift at low N can also be well interpreted by using expression (7). When N decreases to 1, the phase shift $\phi_{R,L}$ drifts oppositely at shorter and longer wavelengths around the Bragg wavelength in the spectrum. This is clearly shown in the inset of Fig. 3(b). The change of the phase shift results in a

corresponding variety of the resonant wavelength.

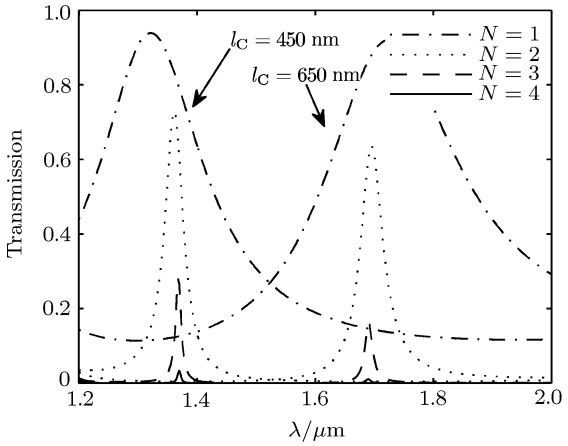


Fig. 8. Transmission spectra of cavity structure $(AB)^N C(BA)^N$ where $l_C = 450$ nm and $l_C = 650$ nm. Other parameters are the same as those in Fig. 4.

To further investigate the resonant properties and provide more information for the optimization design of the SPP cavity, we explore the influence of the insulator thickness d_A on resonant wavelength. The thickness d_A is changed into 70 nm and 30 nm and the corresponding d_B value is increased and decreased to 170 nm and 130 nm respectively, with other parameters remaining unchanged. The transmission spectra are calculated and depicted in Fig. 9 for $N = 2$. It is shown that the peak wavelength is red-shifted with the decrease of d_A, which also accords well with the result in Ref. [23]. Our interpretation is based on resonant condition (7). Changing the insulator thickness into being narrower yields a higher effective refraction index n^{eff} in the MIM waveguide.[17] The higher n^{eff} requires a larger λ in expression (7) to maintain the optical length in the cavity for the resonant condition. In Fig. 9, it is also noted that the transmission peak decreases and narrows down with the insulator thickness d_A decreasing. It means that the decreasing of insulator thickness brings a higher Q value. This result can also be well understood: the decreasing of the insulator thickness results in a deeper contrast between d_A and d_B, which will raise the reflection of the Bragg gratings on the left- and right-hand sides of the cavity. This is clearly demonstrated in Fig. 9 by the broadened forbidden band of $d_A = 30$ nm.

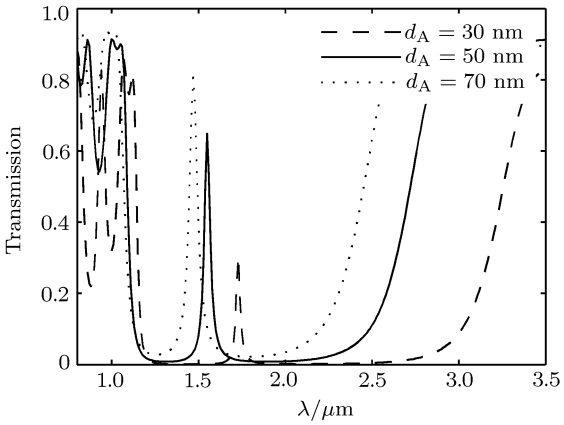


Fig. 9. Transmission spectra of the cavity structure $(AB)^N C(BA)^N$ where $d_A = 30$ nm (d_B=130 nm), $d_A = 50$ nm($d_B = 150$ nm) and $d_A = 70$ nm ($d_B = 170$ nm). Other parameters are the same as those in Fig. 4.

4. Conclusion

We investigate the resonant characteristics and enhancement phenomena of the surface plasmon nanocavity constructed in the thickness-modulated MIM waveguides. The characteristic impedance based TMM is used to calculate the transmission spectrum. The FDTD method is used to simulate the resonant mode and obtain the energy intensity distribution in the cavity. The enhancement of the local field is obvious but limited due to the heat loss from the metal. The changes of the cavity length and thickness give rise to the resonant wavelength shift and a variety of Q values The interpretation based on the Fabry–Pérot resonant theory is given. This treatment could be used to interpret some other similar resonant phenomena in SPP devices. Numerical results for the dependence of the resonant characteristics on the structural parameters are given, which can also be used in the optimization of the surface plasmon nanocavities.

References

[1] Krenn J R 2003 *Nat. Mater.* **2** 210

[2] Maier S A, Kik P G, Atwater H A, Meltzer S, Harel E, Koel B E and Requicha A A G 2003 *Nat. Mater.* **2** 229

[3] Barnes W L, Dereux A and Ebbesen T W 2003 *Nature* **424** 824

[4] Pitarke J M, Silkin V M, Chulkov E V and Echenique P M 2007 *Rep. Prog. Phys.* **70** 1

[5] Zhang H X, Gu Y and Gong Q H 2008 *Chin. Phys.* B **17** 2567

[6] Maier S A, Friedman M D, Barclay P E and Painter O 2005 *Appl. Phys. Lett.* **86** 071103

[7] Ebbesen T W, Genet C and Bozhebolnyi S I 2008 *Phys. Today* **61** 44

[8] Veronis G and Fan S 2005 *Opt. Lett.* **30** 3359
[9] Bozhevolnyi S I, Volkov V S, Devaux E, Laluet J Y and Ebbesen T W 2006 *Nature* **440** 508
[10] Nikolajsen T, Leosson K and Bozhevolnyi S I 2004 *Appl. Phys. Lett.* **85** 5833
[11] Yang P F, Gu Y and Gong Q H 2008 *Chin. Phys.* B **17** 3880
[12] Xue W R, Guo Y N and Zhang W M 2009 *Chin. Phys.* B **18** 2529
[13] Tanaka K and Tanaka M 2003 *Appl. Phys. Lett.* **82** 1158
[14] Liu L, Han Z and He S 2005 *Opt. Express* **13** 6645
[15] Pile D F P, Ogawa T, Gramotven D K, Matsuzaki Y, Vernon K C, Yamaguchi T, Okamoto K, Haraguchi M and Fukui M 2005 *Appl. Phys. Lett.* **87** 261114
[16] Dionne J A, Sweatlock L A, Atwater H A and Polman A 2006 *Phys. Rev.* B **73** 035407
[17] Feigenbaum E and Orenstein M 2007 *J. Lightwave Technol.* **25** 2547
[18] Hobson P A, Wedge S, Wasey J A E, Sage I and Barnes W L 2002 *Adv. Mater.* **14** 1393
[19] Tredicucci A, Gmachl C, Capasso F, Hutchinson A L, Sivco D L and Cho A Y 2000 *Appl. Phys. Lett.* **76** 2164
[20] Wang B and Wang G P 2005 *Appl. Phys. Lett.* **87** 013107
[21] Hosseini A and Massoud Y 2006 *Opt. Express* **14** 11318
[22] Han Z, Forsberg E and He S 2007 *IEEE Photon. Technol. Lett.* **19** 91
[23] Hu B, Liu J, Gu B, Di S, Sun X and Wang S 2007 *J. Opt. Soc. Am.* A **24** A1
[24] Johnson P B and Christy R W 1972 *Phys. Rev.* B **6** 4370
[25] Ramo S, Whinnery J R and Duzer T V 1994 *Fields and Waves in Communication Electronics* (New York: John Wiley&Sons)
[26] Veronis G and Fan S H 2005 *Appl. Phys. Lett.* **87** 131102
[27] Hosseini A, Nejati H and Massoud Y 2008 *Opt. Express* **16** 1475
[28] Kocabas S E, Veronis G, Miller D A B and Fan S 2008 *IEEE Journal of Selected Topics in Quantum Electronics* **14** 1462
[29] Yeh P 1998 *Optical Waves in Layered Media* (New York: Wiley)